SUPPORTING INFORMATIONS

High-toughness, Extensile and Self-healing PDMS Elastomers Constructed by Decuple Hydrogen Bonding

Jing-Han Gao, Baoquan Wan, Ming-Sheng Zheng, Longbo Luo, Hongkuan Zhang, Quanliang Zhao*, George Chen, Jun-Wei Zha**

Experimental Section

Materials

Bis(3-aminopropyl) terminated poly(dimethylsiloxane) (H_2N-PDMS-NH_2, Mn=5000) was obtained from Meryer (Shanghai) Chemical Technology Co., Ltd. Carbohydrazide (CHZ) and hexamethylene diisocyanate (HDI) were purchased from Aladdin Reagent (Shanghai) Co., Ltd. Tetrahydrofuran (THF) was obtained from Beijing Lanyi Chemical Product Co., Ltd. Dibutyltin dilaurate was purchased from Shanghai Macklin Biochemical Co., Ltd. Carboxylated carbon nanotubes (CNTs, OD = 20–30 nm, length = 10–30 μm, 99%) were provided by Jangsu XFNANO Technology Co., Ltd.

Fabrication of prepolymers

NH_2-PDMS-NH_2 was dissolved in dried THF under continuous stirring. HDI was then added. The mixture solution was continuously stirred at 25 °C in a N_2 atmosphere for 24 h to obtain the prepolymers.

Synthesis of CHZ-PDMS

CHZ and dibutyltin dilaurate were added into the prepolymer solution and stirred at 40 °C for 12 h. Then the mixture was introduced into a polytetrafluoroethylene mold and dried at room temperature for 48 h. After evaporation of THF, the CHZ-PDMS elastomer was obtained by peeling off the elastomer from the polytetrafluoroethylene mold. The ratio of CZH and HDI in CHZ-PDMS-1 was 0.125, in CHZ-PDMS-2 was

0.25 and in CHZ-PDMS-3 was 0.375.

Preparation of CNTs/ CHZ-PDMS-2

Firstly, the carboxylated CNTs were dissolved in THF solution with alternating 2 h of sonication and 30 min of stirring for a total of 12 h. Then, the dispersed solution was added to the CHZ-PDMS-2 solution. Mixed solution was alternately stirred and sonicated for 12 h. Finally, the CNTs/CHZ-PDMS elastomer was obtained by peeling off the elastomer from the polytetrafluoroethylene mold. The 5 wt%, 10 wt%, 15 wt% and 20 wt% CNTs/CHZ-PDMS were successfully prepared.

Fabrication of soft strain sensors and devices for electrocardiogram (ECG) and electromyogram (EMG)

Conductive silver paste was applied on the contact section between wire and 15wt%-CNTs/CHZ-PDMS-2 to ensure good electrical contact between the specimen and the electrodes. When the conductive silver paste solidified, a silicone adhesive was subjected to enhance the connection. 15wt%-CNTs/CHZ-PDMS-2 were cut into the shape of electrodes and then bonded to the electrode substrate with conductive gel. The prepared electrodes were connected with the electrode base. The electrode device was fixed to the volunteer's body through proof fabric.

Fourier transform infrared (FTIR) spectroscopy

FTIR spectra of the prepolymer and the CHZ-PDMS samples were recorded on an attenuation total reflectance Fourier-transform infrared spectroscopy (ATR-FTIR, BRUKER TENSOR 27 Spectrometer) with a scanning resolution of 8 cm^{-1} and 32 scanning times. Variable temperature FTIR spectra test was raised from 25 ℃ to 145 ℃ at a heating rate of 3 ℃·min^{-1}, the spectra every 10 ℃ were recorded.

^{1}H nuclear magnetic resonance (NMR) spectroscopy

NMR spectra were recorded in a BRUKER AVANCE 400 using the solvent of

chloroform-d (CDCl3, Sigma-Aldrich) with tetramethylsilane (TMS) as the internal reference.

Thermogravimetric analysis (TGA)

TGA was conducted by using a SDT Q600 tester to test the thermostability of elastomers. The samples were heated from 30 ºC to 800 ºC with a heating rate of 10 $^{o}C \cdot min^{-1}$ in the nitrogen atmosphere.

Differential scanning calorimetry (DSC)

DSC curves were carried by a NETZSCH thermal analyzer (DSC 60) at a heating rate of 10 ℃/min from -140 ℃ to 80 ℃ under liquid nitrogen.

Dynamic mechanical analysis (DMA)

DMA was implemented on Hitachi DMA7100 recorded from 25 to 120 °C by 5 °C/min, with a frequency of 1 Hz.

Mechanical tests

The mechanical properties of different samples were measured by a tensile testing machine (ESM303) with a loading rate of 13 $mm \cdot min^{-1}$ at room temperature. Each sample was tested at least three times. Toughness is the integrating area of the stress-strain curve. All the films were cut into 1cm ×5cm samples for mechanical tests.

Self-healing capability tests

The samples were cut into two pieces by using a clean blade, and then the fracture surfaces of the two parts were contacted to repair in different temperature and repair for different times at 80 ℃. The optical microscope (XSP-002) was used to observe the change of the fracture surface in the repaired samples. The scanning electron microscope (FESEM-SU8010, Hitachi) was used to observe the change of the fracture section in the repaired samples. The healed samples were stretched following the above-mentioned procedure on the ensile testing machine (ESM303) to obtain the stress–strain

curves. The mechanical self-healing efficiency (η) was defined as the ratio of the restored toughness to the original toughness.

Diffraction of x-rays (XRD) testing

Diffraction of x-rays spectra were obtained on Netherlands Panalytical at a scan speed of 10 °·min^{-1}.

Atomic force microscopy (AFM)

AFM was conducted using Bruker Dimension Icon.

Small-angle X-ray scattering (SAXS)

In-situ SAXS experiments were conducted in Anton Paar SAXSess MC2.

The domain distance (d) was calculated from Bragg's law,

$$d = \frac{2\pi}{q_{max}}$$

Density Functional Theory (DFT) simulations

The present DFT simulations were performed with Dmol3 module in BIOVIA Materials Studio simulation package.

In this work, the electron interactions were described with DFT semi-core pseudo potentials, and the exchange correlation energy was evaluated by means of the generalized gradient approximation (GGA) with parametrization of Perdew-Burke-Ernzerhof (PBE). The basis set was set to DNP 4.4. The Convergence energy was set to 10^{-5} Ha (1Ha=27.211eV) and the self-consistent field tolerance to 10^{-6} Ha atom^{-1}.

The simulation super cells for the DFT calculations were constructed with orthodromic symmetry consisting the a, b and c dimensions that were set to 11, 23and 27Å for the small (quadruple HB) and 11, 21 and 50Å for the large molecules (octuple HB). Both molecules were inserted in the center of the cell and surrounded with vacuum to prevent mutual interactions between the adjacent cells due to the periodic boundary conditions. Before any tensile tests, the atomic positions in all simulation cells were optimized

according the mentioned criteria.

In the present DFT simulations, we paid our attention to the hydrogen bonds and their strength between both molecules located in individual simulation cells. Here, we must highlight that both molecules were bonded to each other due to these hydrogen connections. These bonds were tested with respect to their strength via the following deformation procedures. The first procedure consisted simple tension, i.e. the upper molecule was moved as a rigid block from the bottom one. The movement was realized via the incremental shifts of 0.1 or 0.2 Å. The bonding force between molecules was determined from the total energy changes with respect to the deformation (shift).[1] Basic principles of these methods are depicted.

Tests of sensors

Electrical conductivity and sheet resistance of the MGNF were measured by a four-probe method (Sevenstar, China, D41-11E/ZM). Relative resistance change(ΔR/R0) is given by ratio of resistance change to initial resistance. The flexible sensing device was placed on the tensile testing machine to test the resistive change during the tensile process. The flexible sensing device was fixed at the wrist joint of the body, and the change of the resistance with the bending angle was measured. For the human electrophysiology measurement, the device was bonded to a signal processing device with a wireless module (BMD101, NeuroSky) through a medical adhesive tape (3 M, 2733).

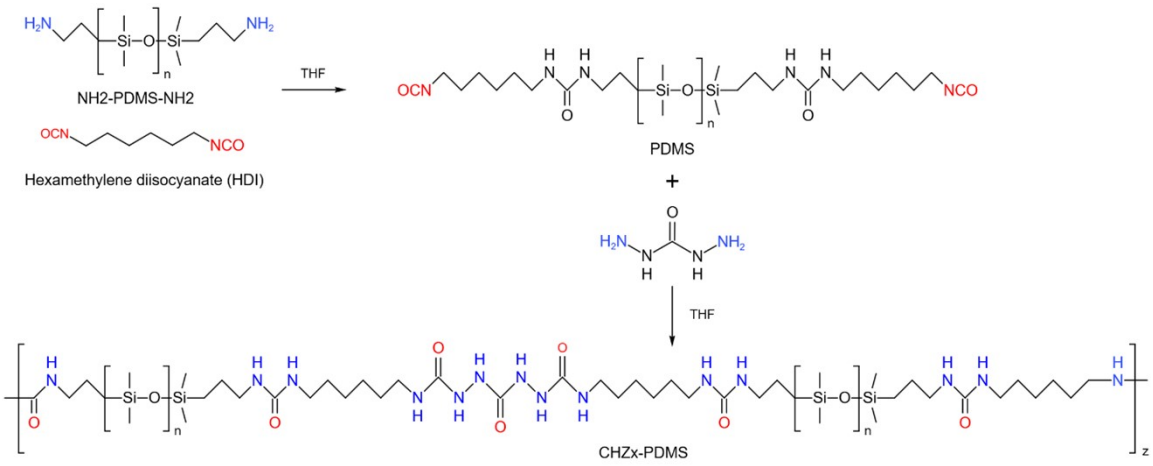

Figure S1. Synthesis process of CHZ-PDMS.

Table S1. The dosage of raw materials and molecular weight of elastomers.

	NH_2-PDMS-NH_2(mmol)	HDI(mmol)	CHZ(mmol)	Mn
PDMS-0	2.0	2.0	0	13218±16.119%
CHZ-PDMS-1	1.75	2.0	0.25	11897±13.822%
CHZ-PDMS-2	1.5	2.0	0.5	10575±10.327%
CHZ-PDMS-3	1.25	2.0	0.75	9253±11.935%

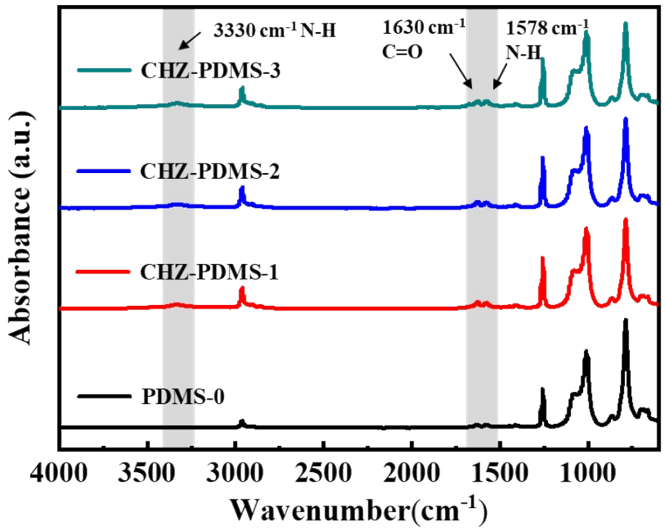

Figure S2. FTIR spectra of PDMS-0 and CHZ-PDMS.

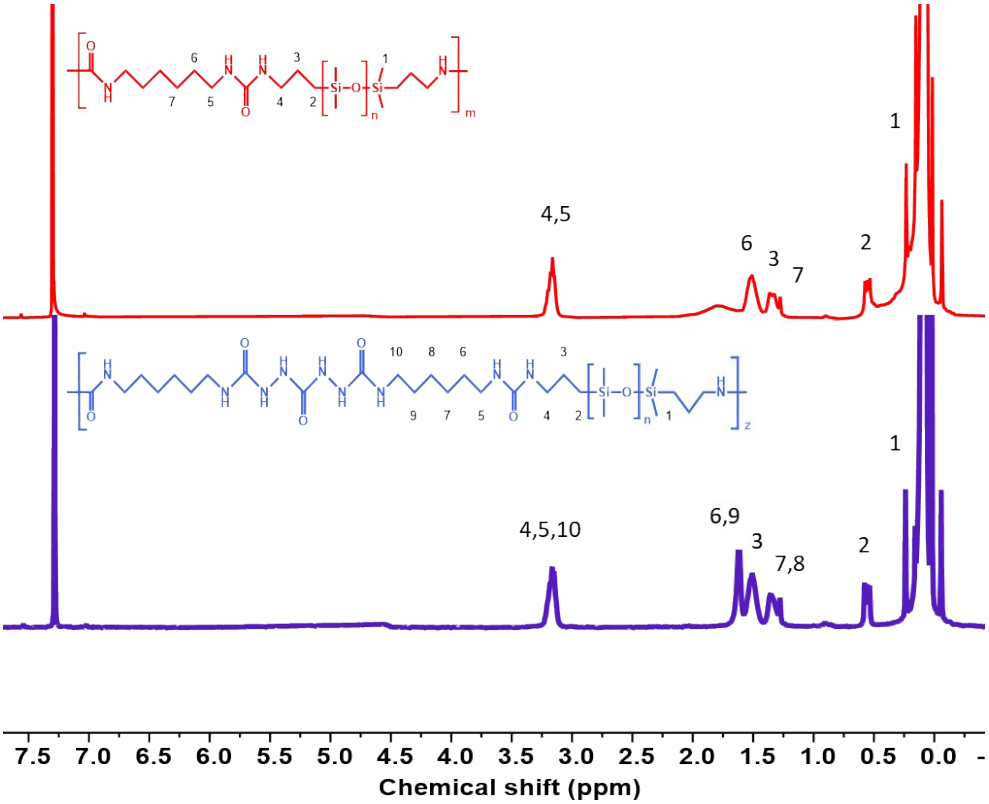

Figure S3. ^{1}H NMR spectra of PDMS-0 and CHZ-PDMS-2.

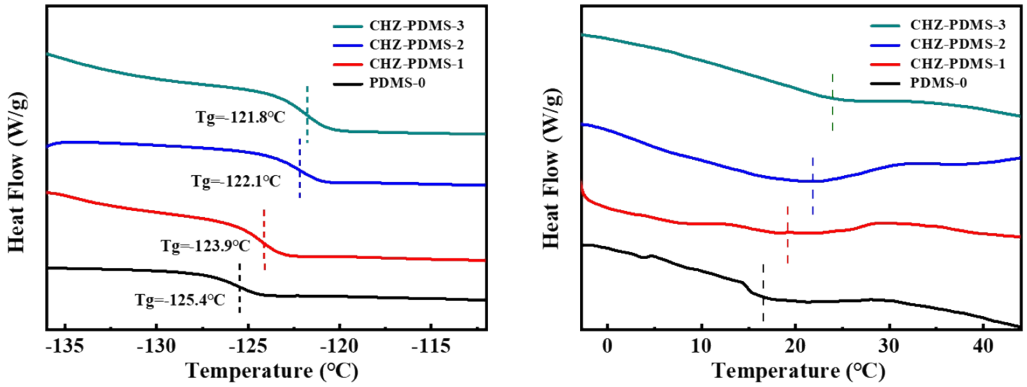

Figure S4. DSC curves of PDMS-0 and different CHZ-PDMS elastomers.

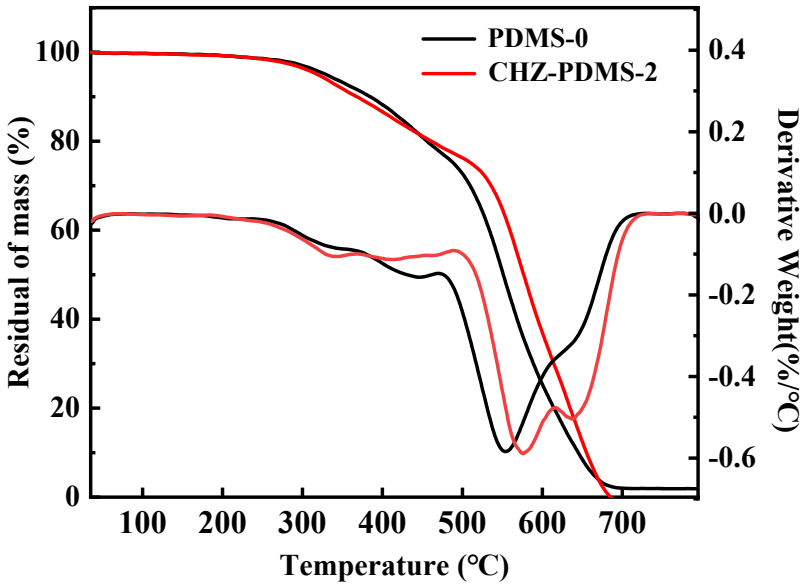

Figure S5. TGA and DTG curves of PDMS-0 and CHZ-PDMS-2.

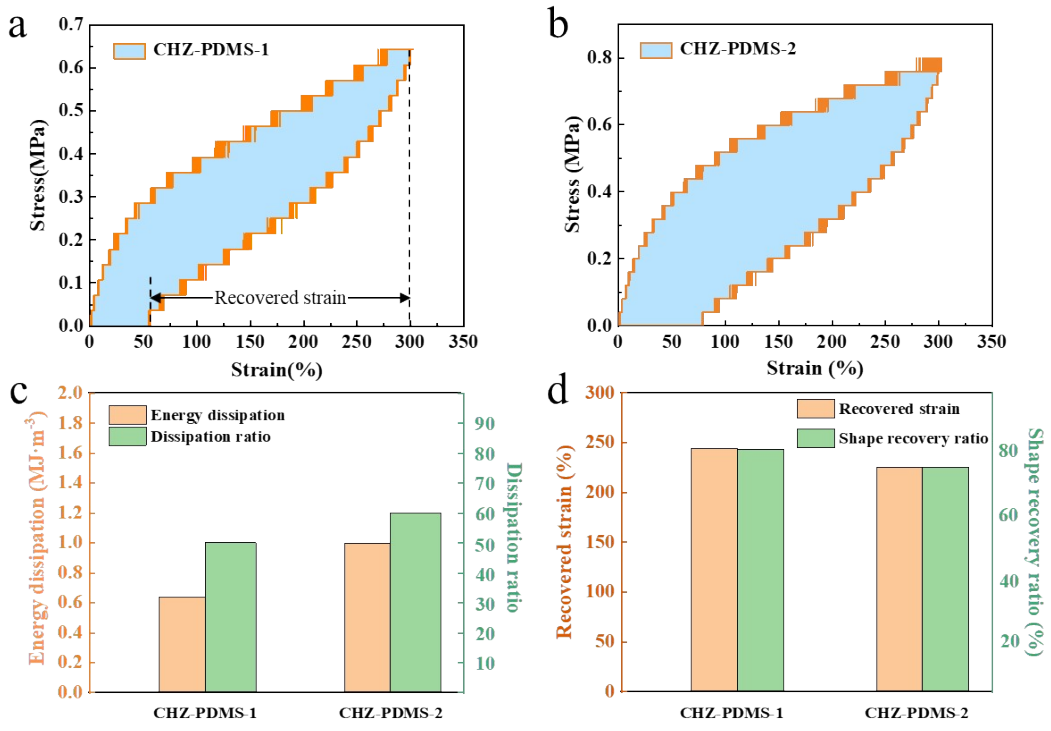

Figure S6. Typical cyclic loading/unloading curves of (a) CHZ-PDMS-1 and (b) CHZ-PDMS-2. (c) Energy dissipation and dissipation ratio of CHZ-PDMS-1 and CHZ-PDMS-2. (d) Recovered strain and shape recovery ratio of CHZ-PDMS-1 and CHZ-PDMS-2. Energy dissipation of tensile cycles is the is the area of the blue, which was

calculated by subtracting the integrated area of the unloading curves from the integrated area of the loading curves. Dissipation ratio is the ratio of the area of the closed curves to the integral area of the loading curves. Recovered strain is shown in Figure S6(a), and shape recovery ratio is the ratio of the recovered strain to the maximum strain.

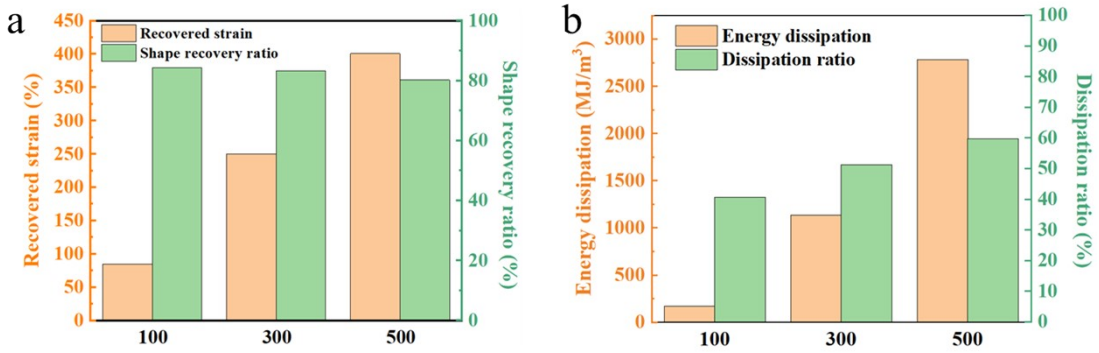

Figure S7. (a) Energy dissipation and dissipation ratio of CHZ-PDMS-2 with different strains. (b) Recovered strain and shape recovery ratio of CHZ-PDMS-2 with different strains.

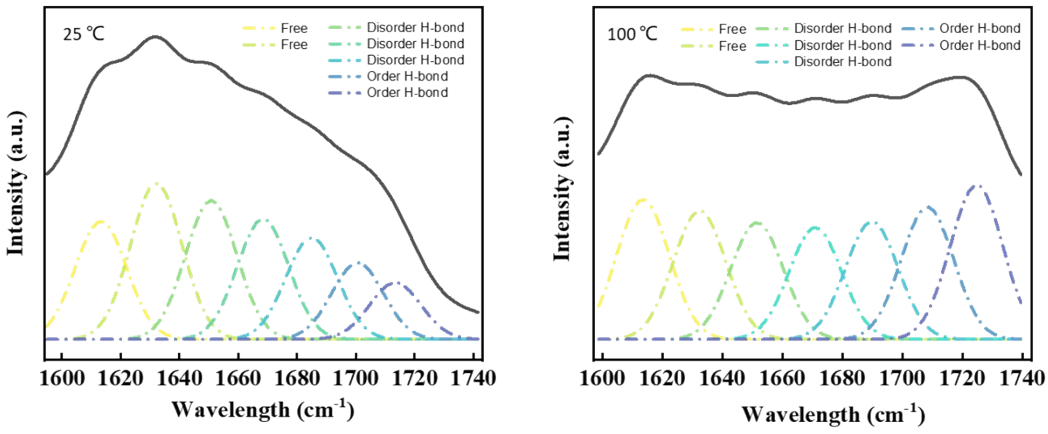

Figure S8. The FTIR spectra of CHZ-PDMS-2 carried out at 25 and 100 °C, respectively.

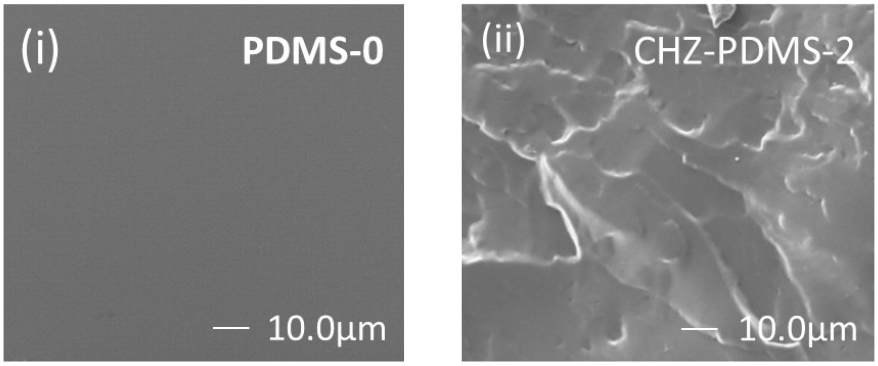

Figure S9. SEM images of (i) PDMS-0 and (ii) CHZ-PDMS-2.

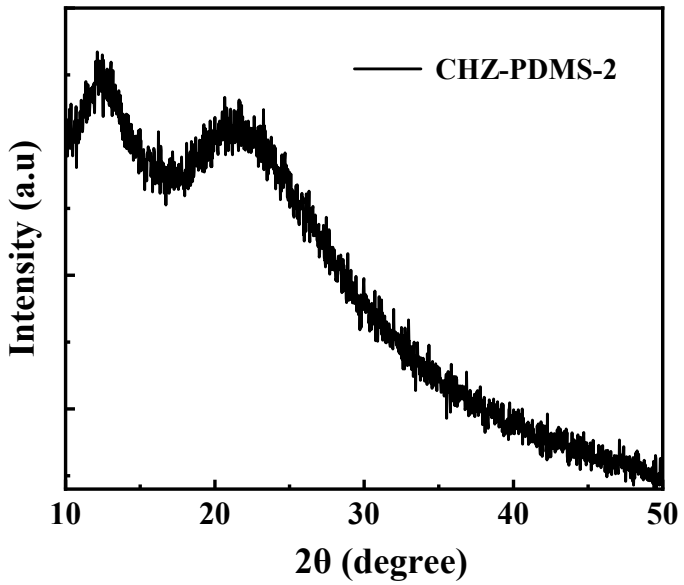

Figure S10. XRD spectra of CHZ-PDMS-2. There is a strong central absorption peak at 2θ=12° and a central absorption broad peak at 2θ=20°.

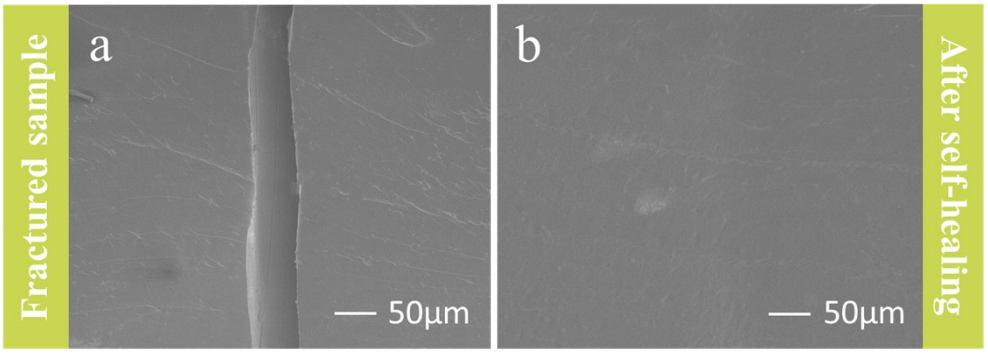

Figure S11. SEM images of lengthwise section of CHZ-PDMS before and after self-healing at 70 ℃. The crack almost disappeared.

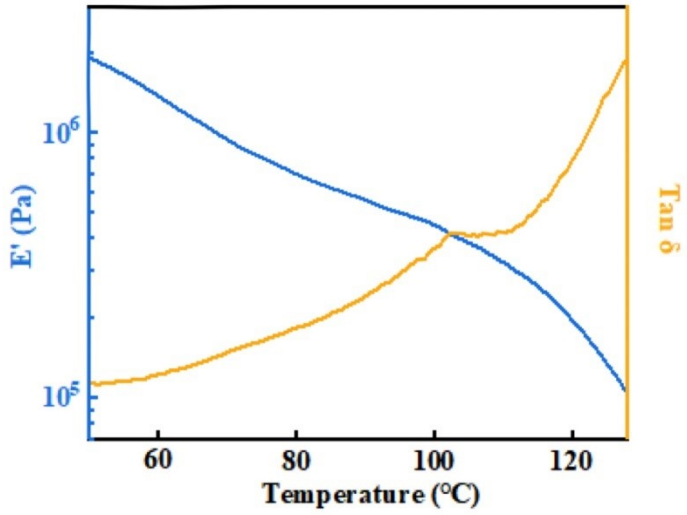

Figure S12. Storage modulus and (d) Tanδ curves of CHZ-PDMS-2.

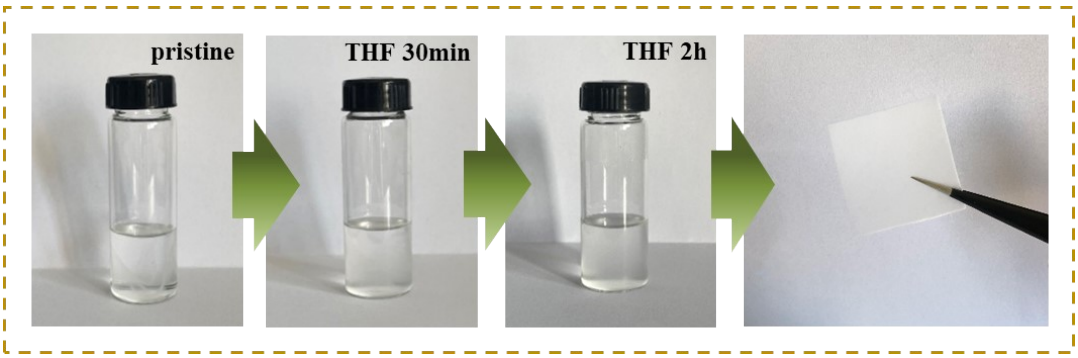

Figure S13. Photographs of pristine CHZ-PDMS and soaked samples after 30 min

and 2 h in THF.

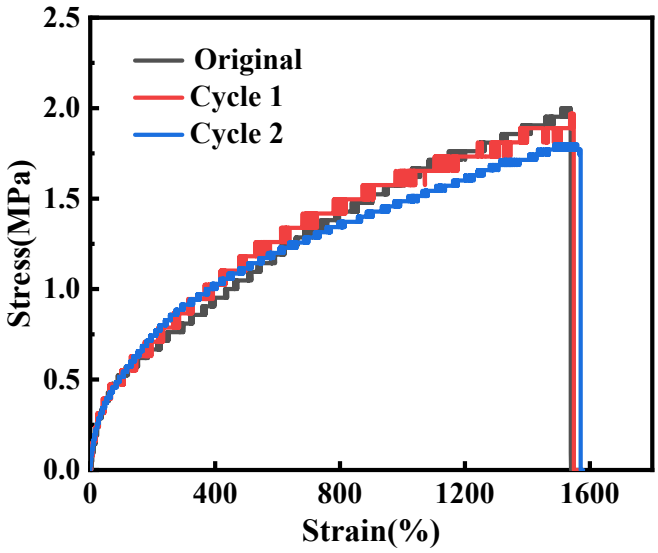

Figure S14. Tensile stress–strain curves of the original and recycled CHZ-PDMS-2 samples.

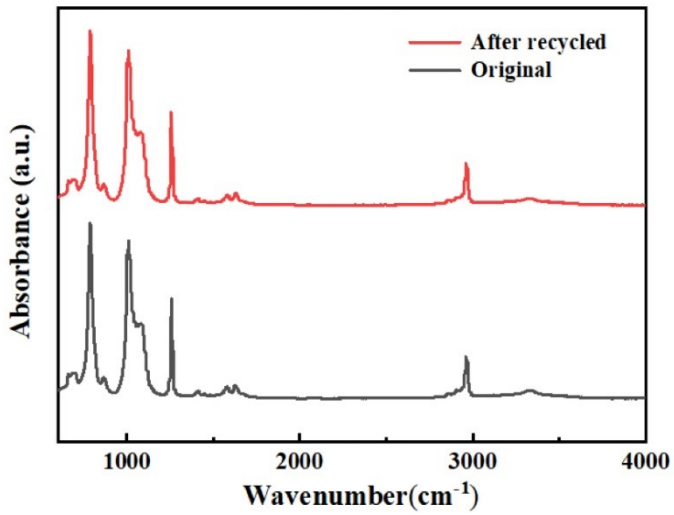

Figure S15. The FTIR spectra of CHZ-PDMS-2 before and after recycling.

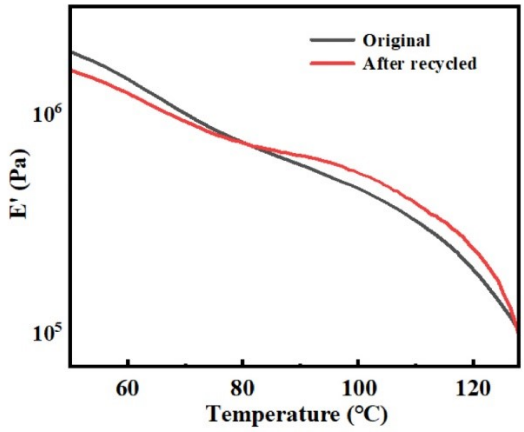

Figure S16. Storage modulus of CHZ-PDMS-2 before and after recycling.

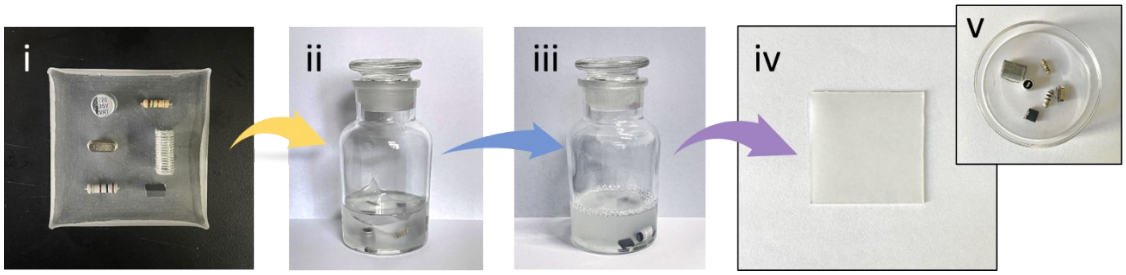

Figure S17. (i) Photos of the device composed by elastomer and electronic components. (ii) and (iii) Dissolution process of elastomer. (iv) and (v) Recycled elastomer and electronic components.

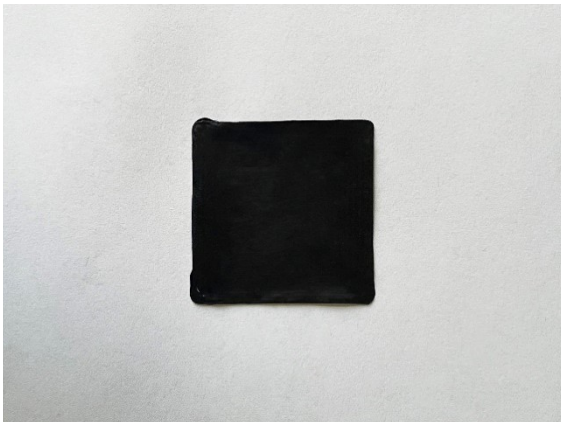

Figure S18. Photos of prepared CNTs/CHZ-PDMS-2 composites.

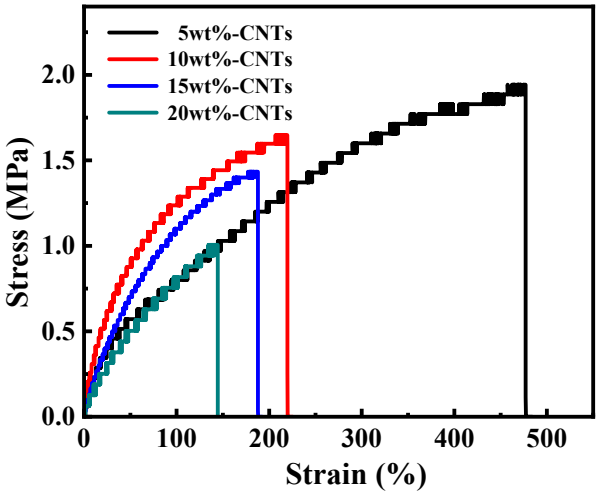

Figure S19. Stress-strain curves of CNTs/CHZ-PDMS-2 conductive composites,

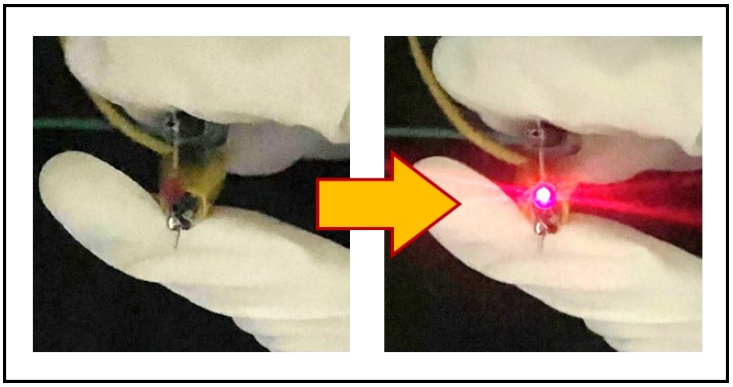

Figure S20. The circuit containing 15%-CNTs/CHZ-PDMS-2 composites can power an LED.

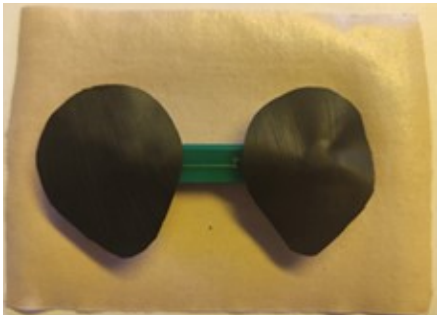

Figure S21. The pictures of electrodes on the wireless module (BMD101, NeuroSky) for electrocardiogram (ECG) and electromyogram (EMG) monitoring.

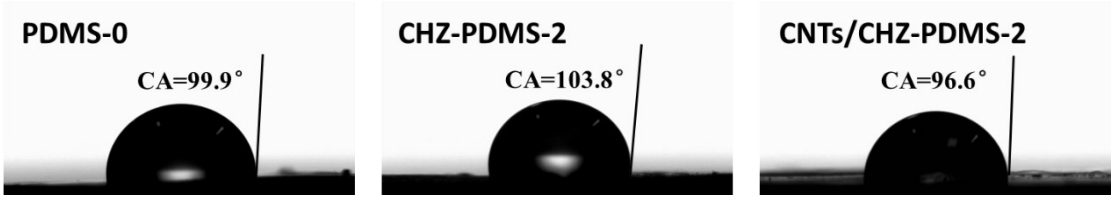

Figure S22. Hydrophobicity tests of PDMS-0, CHZ-PDMS-2 and CNTs/CHZ-PDMS-2.

Table S2. Comparison of performance between CNTs/CHZ-PDMS and other similar PDMS strain sensors. [2-7]

	Strain (%)	GF	Conductivity (S/m)	Self-healing	Hydrophobicity
UCA-2.5@CNT-20 [2]	175%	33.99		Yes	
PDMS-MWCNTs [3]		2			
CNTs/PDMS [4]		1.11			
PDMS/10 wt%MWCNT-Zn^{2+} [5]	169%	3.76		Yes	
PDMS/CNT [6]	350%	20	0.75		
PBS/PDMS-1.5 [7]	105%		2.9×10^{-2}	Yes	
CNTs/CHZ-PDMS-2	186%	20.97	1.12	Yes	Yes

References

[1] Y. Zhuo, Z. Xia, Y. Qi, T. Sumigawa, J. Wu, P. Šesták, Y. Lu, V. Håkonsen, T. Li, F. Wang, W. Chen, Adv. Mater. 2021, 33, 2008523.

[2] D. Mai, J. Mo, S. Shan, Y. Lin, A. Zhang, ACS Appl. Mater. Interfaces. 2021, 13, 49266-78.

[3] C. X. Liu, J. W. Choi, IEEE Trans. Nanotechnol. 2010, 9, 590-5.

[4] D. Guo, H. He, IEEE. In 2018 19th International Conference on Electronic Packaging Technology (ICEPT), Shanghai, China, 8, 2018.

[5] K. Zhang, C. Song, Z. Wang, C. Gao, Y. Wu, Y. Liu, J. Mater. Chem. C. 2020, 8, 17277-88.

[6] R. Zhang, C. Ying, H. Gao, Q. Liu, X. Fu, S. Hu, Compos. Sci. Technol. 2019, 171, 218-25.

[7] P. Qu, C. Lv, Y. Qi, L. Bai, J. Zheng, ACS Appl. Mater. Interfaces. 2021, 13, 9043-52.